JOURNAL OF CATALYSIS 63, 404–414 (1980)

Iron Alloy Fischer–Tropsch Catalysts

II: Carburization Studies of the Fe–Ni System

E. E. UNMUTH,[1] L. H. SCHWARTZ,[2] AND J. B. BUTT[3]

Ipatieff Laboratory, Northwestern University, Evanston, Illinois 60201

Received July 27, 1979; revised December 27, 1979

The formation of carbides on a series of Fe/SiO_2, Ni/SiO_2, and $4Fe:Ni/SiO_2$ catalysts has been investigated in both isothermal (255°C) and temperature-programmed (25–600°C) experiments. Both CO and $3H_2$:CO were employed as reaction gases. With the exception of Ni/SiO_2 in $3H_2$:CO, carbide formation was observed in all instances, although Fe/SiO_2 in CO was incompletely carburized under the conditions of the experiments. Decomposition of Ni_3C formed with Ni/SiO_2 was noted above 350°C; however in the bimetallic catalyst the mixed-metal carbide formed (M_2C to M_3C) was stabilized to about 500°C. In $3H_2:CO$ the rates of carbide formation and coking on $4Fe:Ni/SiO_2$ are both enhanced relative to Fe/SiO_2. A surface reaction model accounting for the observed carburization behavior and in agreement with activation energy measurements is proposed.

INTRODUCTION

Recent investigations in this laboratory and elsewhere have shown that reduced iron is not a very active synthesis catalyst and that an activation period is accompanied by carburization of the metallic phase (*1–3*). While it is not yet clear precisely what role carbides play in the synthesis catalysis, their formation at least has a profound effect upon the iron environment (*1*), and a number of prior studies concerning the effects of support interaction, alkali promotion, and alloying have apparently not taken this carburization into account.

In Part I (*4*), we reported the oxidation–reduction behavior of three catalysts, Fe/SiO_2, $4Fe:Ni/SiO_2$, and Ni/SiO_2, all with a total metal loading of approximately 5 wt%, supported on a wide pore silica gel (Davison 62, pore diameter ~15 nm). Characterization techniques employed were Mössbauer effect spectroscopy (MES), X-ray diffraction (XRD), and temperature-programmed gravimetry. This paper treats results obtained by the same methods for the reactions on these catalysts in flowing CO or $3H_2 + CO$ at 1 atm.

CARBIDES OF IRON AND NICKEL

Iron forms a variety of carbides distinguished from one another by their crystallographic and magnetic differences. The crystal structures are very similar: iron atoms are distributed in a nearly close-packed array, either fcc or hcp, with the carbon atoms in one of several ordered arrangements on the interstices. The phase change from one carbide to another requires only small changes in iron positions and carbon stoichiometry (*5*), and phase identification via X-ray diffraction for supported small particles, as involved here, is difficult. Hence, detection of the magnetic properties, particularly via the Mössbauer effect, is the most sensitive means of phase identification. Arents *et al.* (*6*) have characterized the local magnetic structures of the various carbides using Mössbauer spectroscopy; their results are listed in Table 1 with the appropriate crystallographic data. For a list of original source references, see (*6, 7*).

[1] Present address: Amoco Oil Company, Naperville, Illinois 60540.

[2] Department of Materials Science and Engineering, Materials Research Center.

[3] Department of Chemical Engineering; to whom correspondence should be addressed.

0021-9517/80/060404-11$02.00/0

TABLE 1

Iron Carbides

Carbide	Crystal structure	Curie temperature (°C)	Magnetic iron positions	H (kOe)	Relative population of position	Formula	Lattice constants (Å)
ϵ	hcp	380 ± 10	I	170 ± 3	4	Fe_2C	a = 4.767[a]
			II	237 ± 3	1.6		b = 4.354[a]
			III	130 ± 6	1		a = 2.73[b]
							b = 4.33[b]
ϵ'	Transition from hcp to monoclinic	450 ± 10	I	170 ± 3	—	$Fe_{2.2}C$	—
χ	Monoclinic	232 ± 10	I	184 ± 3	2	Fe_5C_2	a = 11.562
			II	222 ± 3	2		b = 4.5727
			III	110 ± 6	1		c = 5.0595
							β = 97.74°
χ'	Transition from monoclinic to orthorhombic	220 ± 10	I	203 ± 3	2	—	—
			II	214 ± 3	1.8		
			III	118 ± 6	1		
χ''	Transition from monoclinic to orthorhombic	210 ± 10	I	195 ± 3	1	—	—
			II	212 ± 3	2		
			III	118 ± 6	1		
θ	Orthorhombic	208 ± 3	I	208 ± 3	1	Fe_3C	a = 5.0896
			II	208 ± 3	2		b = 6.7443
							c = 4.5248

[a] From Nagakura (*9*).
[b] From Hofer *et al.* (*13*).

As shown in Table 1, the ϵ, χ, χ', and χ'' iron carbides each contain three magnetically nonequivalent iron environments which give rise to three distinct six-line spectra in the Mössbauer pattern, while the ϵ' and θ appear as single six-line patterns. The identification of the carbide phase present is then based on the number of six-line spectra observed, their hyperfine magnetic field (H), and the relative intensities of these spectra.

The relative stability of the various carbides is apparently affected by the ratio of H_2 to CO in the carburization gas (*8, 9*), particle size and strain (*6*), and the amount of initially reduced iron (*10, 11*). Evidence for the presence of various carbides in used synthesis catalysts may be found in (*6, 7, 10*).

Nickel carbide (Ni_3C) has a close-packed hexagonal arrangement of nickel atoms (*12*) and can be prepared by carburization in CO above 200°C (*12–14*). Hofer *et al.* (*13*) point out that below 270°C almost pure carbide is formed in CO, while above that temperature the carbide formation is accompanied by coking; decomposition has been observed at temperatures as low as 380–420°C (*12*). Tøttrup (*14*) used X-ray diffraction to study Ni/η-Al_2O_3 carburized in CO and found Ni_3C with some elemental Ni and C between 300 and 340°C, but only elemental Ni and C above 360°C.

Nickel carbide and iron carbide are completely soluble in one another, but the stability of the mixed carbide decreases with increasing nickel content (*15*). The mutual solubility is due in large part to the similarity between the two carbide crystal structures, both being based on close-packed

layers of metal atoms with ordered arrays of carbon in the metal interstitial positions. The lattice constants for the arrangement in Ni_3C are a = 2.6502 Å, and c = 4.3383 Å, while in the hexagonal ϵ-Fe_2C, a = 2.73 Å and c = 4.33 Å (*15*). The addition of carbon to an iron–nickel alloy tends to stabilize the fcc phase over the bcc phase; in fact, the packing of the ϵ-Fe_2C iron atoms is very similar to the fcc metal packing.

EXPERIMENTAL

Catalysts. The catalysts were prepared by impregnation of 80- to 100-mesh Davison 62 silica gel to incipient wetness with the appropriate aqueous solution of the nitrate salt. Simultaneous impregnation was used in preparation of the bimetallic. A complete description of the details of preparation and characterization of the catalysts investigated here is given in Part I (*4*).

Characterization. Characterization via Mössbauer spectroscopy, X-ray diffraction, and temperature-programmed gravimetry also has been described in Part I (*4*), and complete details are given by Unmuth (*7*). The temperature-programmed carburization (TPC) experiments were conducted in both CO and $3H_2$:CO over the same range of programming rates, 5–25°C/min, and temperatures, 25–600°C, as the oxidation–reduction studies. Sample pretreat procedures were also the same, except here the initial sample was the reduced metal (H_2, 425°C, 24 hr and then H_2, 485°C, 0.5 hr immediately prior to the experiment). Also as in the case of the oxidation–reduction studies, a number of carburization experiments were run isothermally at ca.255°C.

RESULTS

Fe/SiO_2. The TPC profiles for the reaction of Fe/SiO_2 in flowing CO are shown in Fig. 1 for three programming rates. The three separate peaks observed will be referred to as α, β, and γ. If all the reduced iron were completely carburized, the maximum C/Fe ratio attainable would be 0.50 (assuming the formation of Fe_2C). In fact observed C/Fe ratios for the β and γ peaks varied from 0.79 to 1.48 depending upon temperature-programming rate, with a total accumulation of 1.85–2.32 mol C/mol reduced Fe at 750°C. It is apparent that this excess carbon is present as a result of coking and the β and γ peaks are assigned to this process. A TPC experiment was terminated after the α transition and the resulting sample examined with MES and XRD. Both techniques indicated incomplete carburization with the spectra dominated by that from iron metal. The carbide that was present was of sufficiently small size to be superparamagnetic at room temperature, and no distinction between the various carbides could be made from either the MES or XRD results.

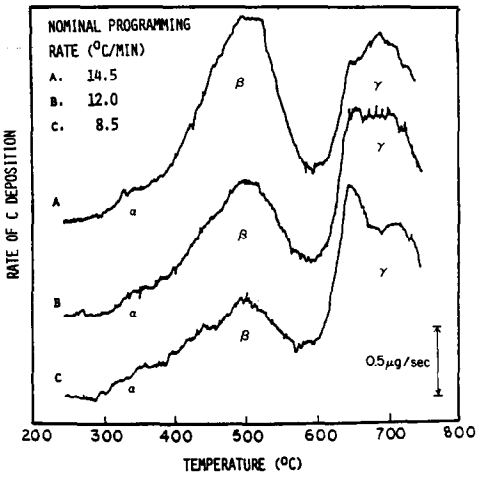

FIG. 1. TPC of Fe/SiO_2 in CO.

Remarkably different results were obtained for TPC with flowing $3H_2$:CO as shown in Fig. 2. The α peak is now much more clearly resolved and the β and γ peaks have increased in rate by a factor of 3–4. The latter was again associated with coking and resulted in C/Fe ratios of 8.2–12.0 at 660°C. The C/Fe ratio for the α peak was determined and is given in Table 2. It is seen that this ratio is less than that expected for the lowest carbide (Fe_3C) imply-

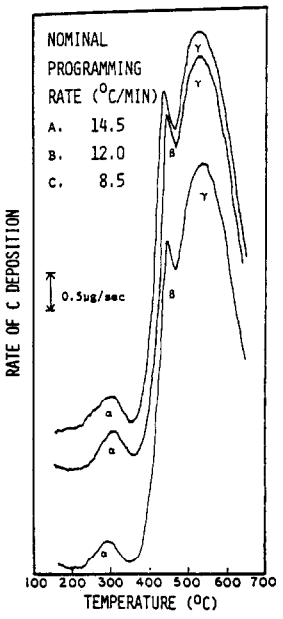

FIG. 2. TPC of Fe/SiO_2 in $3H_2$:CO.

ing either a highly nonstoichiometric carbide or, more likely, incomplete carburization. However, the extent of carburization determined from MES after the α transition in the synthesis mixture was much greater than in carbon monoxide alone, as was the amount of coke determined gravimetrically. Clearly hydrogen facilitates both carbon deposition and carbide formation on iron catalysts, suggesting that hydrogen participates in (or influences) the rate-limiting steps for both of these processes.

TABLE 2

C/Fe Ratio for the TPC of Fe/SiO_2 in $3H_2$:CO, α Peak[a]

Profile	Programming rate (°C/min)	Mol C/mol Fe
A	14.5	0.27
B	12.0	0.19
C	8.5	0.22
Fe_3C	—	0.33
Fe_2C	—	0.50

[a] Based on an assumed 90 at.% reduced iron, initially.

Isothermal carburizations were carried out at 256 ± 2°C using both the synthesis mixture $3H_2$:CO and CO. The observation from TPC that carburization is more rapid and more complete in the synthesis mixture was confirmed in these experiments as illustrated in Fig. 3. Mössbauer spectra of samples which have passed the α transition indicate incomplete carburization in the case of pure CO and complete carburization in $3H_2$:CO. Studies to determine the carbide phases formed under these conditions are currently underway. The C/Fe ratios after 3 hr of carburization in CO and $3H_2$:CO were 0.23 ± 0.01 and 0.41 ± 0.01, respectively, corresponding to 51 at.% iron as carbide in the former case and 90–98 at.% iron as carbide in the latter; the range results from the need to assume a ratio of χ to ϵ' phases.

Ni/SiO_2. TPC studies of Ni/SiO_2 in flowing CO are acharacterized by three regimes as shown in Fig. 4. XRD patterns from samples removed after the α, β, and δ transitions confirmed the presence of Ni_3C after the α transition, while only elemental Ni was detected after the β and δ transitions. The decomposition of Ni_3C in the β transition occurs at a surprisingly high temperature. When this temperature, T_β, is linearly extrapolated to zero programming rate, a transition temperature of 428°C is obtained, much higher than the 360°C reported by Tøttrup (*14*) for Ni/η-Al_2O_3. The

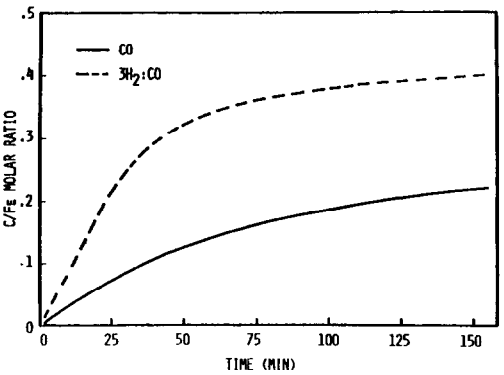

FIG. 3. Isothermal carburization of Fe/SiO_2 at 256 ± 2°C.

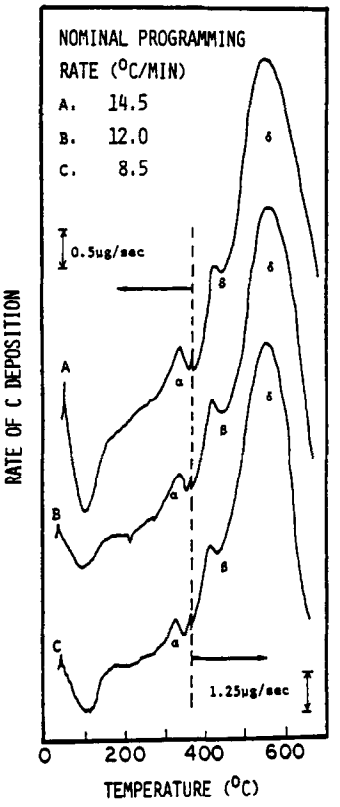

FIG. 4. TPC of Ni/SiO_2 in CO.

C/Ni ratios for the α transition were 0.32, 0.31, and 0.35 (all ± 0.01) for the three programming rates displayed in Fig. 4, in excellent agreement with expectation for Ni_3C and indicative of complete carburization of Ni in CO for this temperature regime.

By contrast, attempted carburization of Ni/SiO_2 in TPC experiments in flowing $3H_2$:CO produced only apparent weight changes due to buoyancy effects. No carbide or coke was observed at the partial pressure of hydrogen used. Since nickel carbide is easily reduced to methane and elemental nickel in hydrogen (*10, 16, 17*), it seems clear that any carbon formed by CO dissociation rapidly reacts with hydrogen to form methane in these experiments.

Isothermal carburization of Ni/SiO_2 at 256 ± 2°C is summarized in Fig. 5. For both feeds a small but rapid initial weight gain was noted (C/Ni $\approx$ 0.1). A similar effect was noted upon exposure of the Ni/SiO_2 to these gases at room temperature and may be identified as adsorption. There is no way to verify whether the adsorption is associative or dissociative in this experiment, but at 256°C it is likely that for CO alone the adsorption is dissociative. For the synthesis gas, Storch *et al.* (*18*) have proposed that carbon monoxide and hydrogen form a surface enol group when coadsorbed on Group VIII metals. The extent of hydrogen coadsorption could not be investigated here owing to the very small sample size and associated small weight change. Carburization in CO proceeded rapidly, exceeding the C/Ni ratio for Ni_3C after 50 min. Further carbon weight increase after this time is attributable to coking. The C/Ni ratio after 3 hr was 0.41 ± 0.01, suggesting at least 20 at.% of the carbon in the form of coke. An XRD pattern of this sample confirmed the presence of only Ni_3C. Exposure of the Ni/SiO_2 catalyst to the synthesis gas mixture resulted in very little weight change after the initial rapid adsorption, and the XRD pattern for this sample after exposure for 125 min. showed only nickel metal.

4Fe:Ni/SiO₂. the starting material was prereduced 4Fe:Ni/SiO_2, which consisted of biphasic alloy particles with approximately 23 at.% fcc (containing 37.5% Ni) and 73 at.% bcc (containing 14% Ni) (*4*).

Three peaks were observed in the TPC of

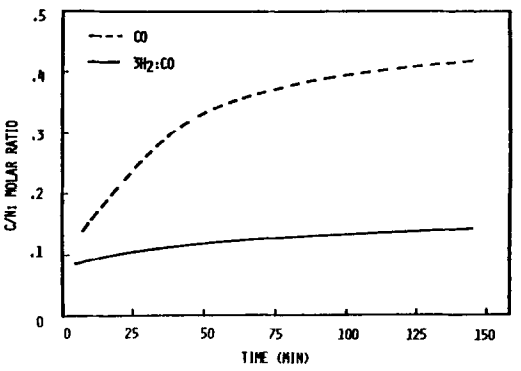

FIG. 5. Isothermal carburization of Ni/SiO_2 at 256 ± 2°C.

$4Fe:Ni/SiO_2$ in CO. The results are displayed in Fig. 6 for the slowest programming rate in comparison with those for Ni/SiO_2 and Fe/SiO_2. Inspection reveals that the behavior of the bimetallic is not that of an equivalent mixture of separate pure-metal catalysts. Only the α peak appears similar; MES of this material indicated a similar but somewhat broader pattern than for Fe/SiO_2 after the α transition, indicative of mixed-metal carbide formation. The carbon to metal ratio at α was 0.38–0.40, corresponding to a stoichiometry intermediate between M_2C and M_3C, and the rate of coking on the bimetallic catalyst is the same as for nickel but at 100°C lower. A MES spectrum of a TPC sample of $4Fe:Ni/SiO_2$ after the δ transition in CO indicated iron still present as carbide; however, it was not possible to determine whether Ni was present as the metal or the carbide.

It has been observed (*19, 20*) that coke formation on iron and metal proceeds by the growth of graphite whiskers. If diffusion thorugh the solid is kinetically important, then crystal structure would be expected to play a major role. In the present instance, the metallic close-packed lattice, expanded by interestitial carbons to form carbide, presents a more open structure enhancing the diffusion of carbon. Thus the higher coking rate on $4Fe:Ni/SiO_2$ compared to either Fe/SiO_2 or Ni/SiO_2 can be explained as a combination of two factors: (i) surface nickel enhancing the rate of dissociation of CO and (ii) carbide providing a more open structure for the transport of carbon to the growing graphite.

The TPC curves for $4Fe:Ni/SO_2$ in $3H_2$:CO were all similar to that shown in Fig. 7. For comparison Fe/SiO_2 results are also shown (recall that Ni/SiO_2 did not carburize in $3H_2$:CO). Rates of both carburization and coking are higher for the bimetallic catalyst, increasing by 50 and 30%, respectively, so the presence of Ni produces a similar effect (increase in both

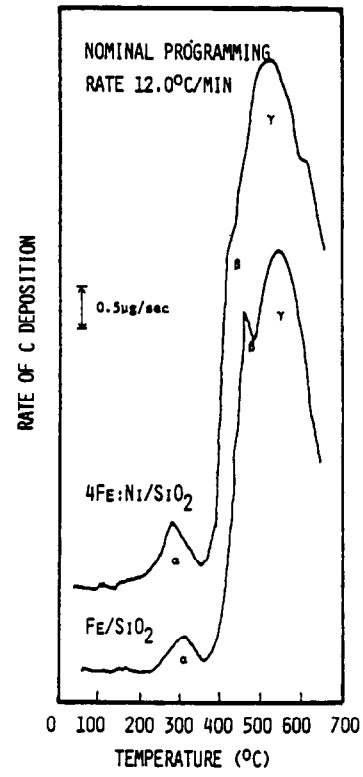

FIG. 7. TPC of Fe–Ni system in $3H_2$:CO.

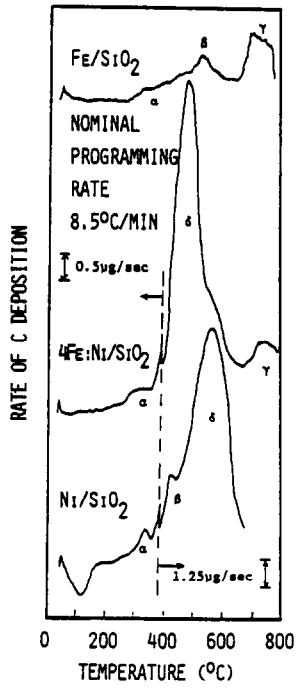

FIG. 6. TPC of Fe–Ni system in CO.

rates) in both atmospheres. The C/metal ratio for α was 0.38 to 0.41 for the range of programming rates, close to that expected for either χ-$Fe_{2.5}C$ or ϵ-$Fe_{2.2}C$. The Mössbauer patterns for samples removed from TPC at the α peak and after 660°C are shown in Fig. 8. At α the spectrum indicates the presence of two carbide phases with hyperfine fields of 185 ± 10 kOe and 159 ± 3 kOe. The major phase (159 kOe) has a hyperfine field that is about 10 kOe lower than that of the ϵ or ϵ' carbide, which is probably a reflection of the modification of the magnetic properties of the carbide via incorporation of nickel. The post 660°C spectrum indicates that the carbide has decomposed to one of the more stable (χ or θ) carbides. Nagakura (*9*) reports the transitions $\epsilon \rightarrow$ (380°)$\chi \rightarrow$ (550°)θ, however the XRD pattern of this material was not consistent with θ-carbide.

Isothermal carburizations were carried out in CO and $3H_2$:CO at 256°C. After 2.5 hr, the carbon to metal ratios were 0.40 and 0.48 for the two gases, respectively. MES analyses of these catalysts were similar to

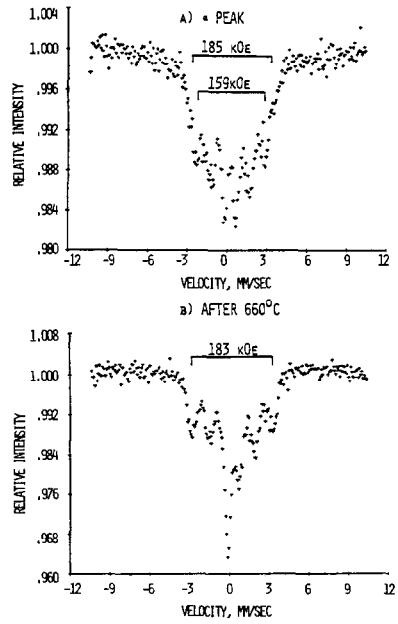

FIG. 8. Mössbauer spectra for the TPC of 4Fe:Ni/SiO_2.

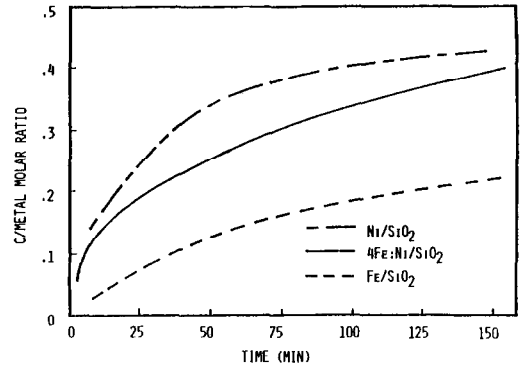

FIG. 9. Isothermal carburization of Fe–Ni system in CO.

those obtained from the TPC samples after the α peak. In the CO atmosphere the catalyst was incompletely carburized, while in $3H_2$:CO essentially complete carburization occurred.

A comparison of the isothermal carburization rates in CO and $3H_2$:CO is shown in Figs. 9 and 10 for the three catalysts examined. Carburization of the bimetallic catalyst in CO is very similar to that of Ni/SiO_2, suggesting that the influence of nickel in dissociating CO is critical in this reaction. On the other hand, in $3H_2$:CO the bimetallic catalyst behaves more like Fe/SiO_2. The high C/metal ratio for 4Fe:Ni/SiO_2 relative to that of Fe/SiO_2 in CO would not be expected on thermodynamic grounds if only carbide formation is considered. It is difficult to say from comparative Mössbauer patterns whether the extent of bulk carbide formation is less in 4Fe:Ni/SiO_2 than in Fe/SiO_2, but certainly the large increase in C/metal ratio in the former case is due to formation of graphite or surface carbide.

Activation energies. Activation energies for the carburizations were determined using the standard temperature-programmed analysis (*21*) requiring a plot of log (PR/T^2) vs ($1/T$), where PR is the programming rate (first-order kinetics assumed), and by an Arrhenius analysis of peak parameters as proposed by Falconer and Madix (*22*). The TPC analysis results were more internally

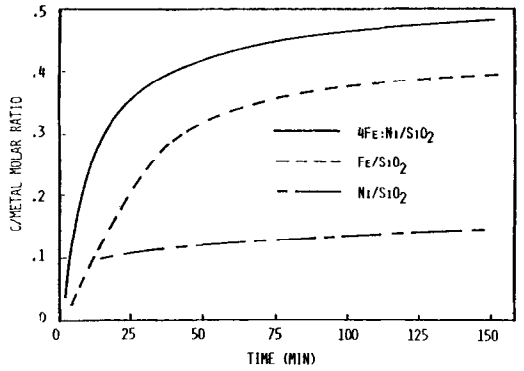

FIG. 10. Isothermal carburization of Fe–Ni system in $3H_2$:CO.

consistent and are reported in Table 3. The large uncertainties indicated for Fe/SiO_2 and $4Fe:Ni/SiO_2$ in CO result from uncertainties in locating the maxima of the weak α peaks for these reactions. In particular the value of 120 kcal/mol for the Fe/SiO_2 in CO is unreasonable in view of the results of Rozovskii *et al.* (*23*) for the carburization of an unpromoted fused iron catalyst in CO (32 kcal/mol). The result for Fe/SiO_2 in the synthesis gas is more precisely determined and, although a bit low, in general agreement with the activation energy for diffusion of carbon in bcc iron, 19.2 kcal/mol (*24*).

The measured activation energy for Ni/SiO_2 in CO, 35 ± 2 kcal/mol, is in excellent agreement with 32.8 kcal/mol reported for the coking of 9.9% Ni/Al_2O_3 in CO (*14*) and 30–34 kcal/mol for coking of nickel catalysts by various hydrocarbons (*20*). The activation energy for diffusion of carbon in nickel has been determined as 33.0 kcal/mol in tracer studies (*24*), suggesting that the solid-state diffusion of carbon through nickel may be rate controlling in coke deposition reactions as well as in the carburization of nickel. The activation energy for the carbide formation of the bimetallic catalyst in $3H_2$:CO was 22 ± 2 kcal/mol, intermediate between that for Fe/SiO_2 and Ni/SiO_2, but there is probably little physical meaning attributable to this number, which represents some sort of average for the carburizations of the bcc and fcc metallic phases.

No activation energies were determined from the TPC in the coking regimes, since the temperature-programmed analysis requires a finite reaction–product relationship. In addition, the temperature ranges here are well beyond those of interest in synthesis reaction applications. One may, however, make some useful generalizations about the coking regimes. The addition of hydrogen to carbon monoxide increased the turnover frequencies and lowered the temperature at which the maximum rate occurred for all the coking and carbide formation peaks of Fe/SiO_2. The same behavior was observed for $4Fe:Ni/SiO_2$. For the case of Ni/SiO_2, coking and carbiding were observed in CO but not in $3H_2$:CO. This similarity between carbide formation and coking implies, at least, that the two processes occur via similar mechanisms.

DISCUSSION

The increase in the rate of carburization and coking of iron-containing catalysts with the introduction of hydrogen to the reaction mixture is strong evidence for the influence of hydrogen on the rate-controlling steps of both processes. Kryukov *et al.* (*25*) have reported the same result for fused iron catalysts and proposed the following explanation. Assuming a composition of Fe_2C for the carbide, we may write the overall chemical reactions in the two atmospheres as

$$2Fe + 2CO \rightarrow Fe_2C + CO_2 \quad (1)$$

$$2Fe + CO + H_2 \rightarrow Fe_2C + H_2O \quad (2)$$

TABLE 3

Activation Energies for the Carburization Reaction

Catalyst	Reaction	E (kcal/mol)
Fe/SiO_2	$Fe + CO \rightarrow Fe_xC$	120 ± 20
	$Fe + CO + H_2 \rightarrow Fe_xC$	14 ± 4
Ni/SiO_2	$Ni + CO \rightarrow Ni_3C$	35 ± 2
$4Fe:Ni/SiO_2$	$4Fe:Ni + CO \rightarrow (4Fe:Ni)_xC$	15 ± 7
	$4Fe:Ni + CO + H_2 \rightarrow (4Fe:Ni)_xC$	22 ± 2

It has commonly been found that CO_2, not water, is the principal oxygen-containing product. However, Kryukov *et al.* reported that the amount of water found in the synthesis product increased with increasing space velocity, an observation consistent only with water being an initial product of reaction; CO_2 could then be produced subsequently by the water gas shift. Hence we may look to Eq. (2) as being important in the carburization under synthesis conditions. If carbon formation is proposed to proceed via a hydrogen–carbon monoxide surface complex, two possible carburization paths are

$$\begin{array}{l} Fe + CO \\ \quad + H_2 \rightleftarrows [FeCO]_s \overset{H_s}{\rightleftarrows} [FeCOH_x]_s \\ \qquad\qquad \downarrow \qquad\quad \downarrow \\ \qquad\quad Fe_2C + CO_2 \quad Fe_2C + H_2O \end{array} \qquad (3)$$

where s indicates an adsorbed state. The hydrogen-containing complex, originally proposed by Storch *et al.* (*18*), was postulated to be the active intermediate for the Fischer–Tropsch reaction; hence carbide formation was seen by Kryukov *et al.* as a side reaction to the major synthesis reactions and the extent of carbide formation dependent upon the ease of abstraction of oxygen from $[FeCOH_x]_s$.

This view, however, neglects the possible dissociation of CO which, if it occurs, could have a large effect on the kinetics of carburization. In fact a great deal of evidence exists for the dissociative adsorption of CO on Group VIII metals (*16, 26–28*). Textor *et al.* (*28*) found for CO on Fe (111) that 85% of the sites were covered by dissociatively adsorbed carbon and oxygen while 15% adsorbed CO molecularly. Dissociative adsorption involves adjacent sites for carbon and oxygen so rates would be governed by the availability of paired sites. Now when carburization is occurring, the carbon so adsorbed is removed from the surface via transport into the metal lattice; hence the rate of removal of oxygen from the surface must be an important factor in determining the availability of paired sites and corresponding surface concentrations of dissociated CO. Thus, in turn it is important that we give consideration to the mechanism of oxygen removal, especially in light of the differences observed here between carburization in CO and CO + $3H_2$. It was reported some time ago (*2, 29*) that there is very little isotopic exchange between carbide carbon and CO during syntheses over iron catalysts and recently Araki and Ponec (*26*) reported the same result for nickel catalysts. Their conclusion is that while there is little likelihood for recombination between surface carbon and oxygen, the surface oxygen could be removed from nickel by reaction with associatively adsorbed CO. The same argument can reasonably be applied to iron as well, and if so the addition of H_2 to CO would certainly facilitate the removal of surface oxygen and enhance the rate of carburization, save for surfaces (e.g., pure nickel in the present case) which are very active hydrogenation catalysts.

For iron, then, we may draw the following picture of carburization in a synthesis gas mixture. At any given time the surface will contain the adsorbed species CO_s, C_s, O_s, and H_s, according to the general reaction model:

$$\begin{array}{l} CO \rightleftarrows CO_s \rightleftarrows C_s + O_s \\ C_s + H_2 \rightleftarrows CH_4 \\ C_s + Fe \rightleftarrows Fe_2C \\ O_s + H_s \rightleftarrows H_2O \\ O_s + CO_s \rightleftarrows CO_2. \end{array} \qquad (4)$$

In the *absence* of hydrogen two steps exist for the removal of both surface oxygen and carbon: the diffusion of carbon into the metal lattice where it reacts to form carbide, and the reaction between oxygen and carbon monoxide to form carbon dioxide. If the rate of dissociative adsorption of CO were high, then either carbon diffusion or oxygen removal could be rate determining in carbide formation. However, it has been well documented (*10*) that iron carbide does not chemisorb significant amounts of

CO, so if there is formed a significant amount of carbide near the surface early in the reaction it is likely that the quantity of associatively adsorbed CO will be small enough to limit the rate of oxygen removal. Further, given the low activation energy and high-frequency factor reported for solid-state diffusion of carbon in iron (*24*) it appears unlikely that this would be rate determining. Unfortunately, as we pointed out previously, the activation energy results obtained here for Fe/SiO_2 in CO are very uncertain and yield no information on the matter.

In the *presence* of hydrogen, though, we have a different situation owing to the possibility of methane and water formation. Unlike CO, hydrogen readily chemisorbs on iron carbide (*10, 18*), facilitating the removal of carbon as well as oxygen from the surface and possibly inhibiting carbide formation. When the hydrogenation of surface carbon is sufficiently rapid, then diffusion of carbon into the metal lattice becomes rate limiting. This view is supported by our experimental results for Fe/SiO_2 in $CO + 3H_2$, where the activation energy was determined more precisely and found to be in agreement with that for diffusion of carbon in bcc iron.

The behavior of the nickel catalyst also conforms to this view. The carburization of Ni/SiO_2, it will be recalled, proceeded rapidly to completion in CO but was inhibited in the synthesis atmosphere. Now nickel is a much better hydrogenation catalyst than iron (*10*) and nickel carbide is much less stable than iron carbide (*15*). This higher probability of carbon hydrogenation coupled with the weaker carbon–metal bond would lead to rates of hydrogenation so much greater than diffusion that the carbide never has the chance to be formed in appreciable quantity. Finally, the fact that nickel carburized more rapidly than iron in CO alone is probably the result of weaker chemisorption of oxygen on the nickel, with consequent more rapid removal via reaction with surface carbon monoxide.

Raupp and Delgass (*3*) have studied small particles of $5Fe:5Ni/SiO_2$ (10% total metals <10 nm) in $3H_2$:CO and found no bulk carburization. On the other hand, samples sintered to form larger particle sizes did show evidence of bulk carburization, however the results were complicated by phase separation during the sintering. They attributed the carburization to the iron-rich bcc phase and concluded that the nickel-rich phase remained uncarburized. Our early results seemed to indicate that both nickel-poor and nickel-rich phases could carburize; however, relative phase identifications via either MES or XRD are inconclusive to date. Aside from particle size effects, alloy composition and total loading may be important in this matter.

ACKNOWLEDGMENTS

The authors are indebted to Dow Chemical, USA, for support of this research through a Dow Chemical Research Fellowship in Catalysis, to support from the Department of Energy, Office of Basic Energy Sciences, Division of Materials Sciences, Contract ER-78-S-02-4493, and to the Northwestern University Materials Research Center, supported by the National Science Foundation—Materials Research Laboratories, Contract DMR 76-80847, in whose Central Facilities the Mössbauer and X-ray studies were performed.

REFERENCES

1. Amelse, J. A., Butt, J. B., and Schwartz, L. H., *J. Phys. Chem.* **82,** 558 (1978).
2. Kryukov, Y. B., Bashkirov, A. N., Liberov, L. G., Butyugin, V. K., Stepanova, N. D., and Kagan, Y. B., *Kinet. Katal.* **1**(2), 274 (1960).
3. Raupp, G. B., and Delgass, W. N., *J. Catal.* **58,** 337, 348, 361 (1979).
4. Unmuth, E. E., Schwartz, L. H., and Butt, J. B., *J. Catal.*, **61,** 242 (1980).
5. Duggin, M. J., *Trans. AIME* **242,** 1091 (1968).
6. Arents, R. A., Maksimov, Y. V. Suydalev, I. P., Imshennik, V. K., and Krupyanskiy, Y. F., *Fiz. Met. Metalloved.* **36,** 277 (1973).
7. Unmuth, E. E., Ph.D. dissertation, Northwestern University, Evanston, Illinois, June 1979.
8. Loktev, S. M., Markarenkova, L. I., Slivinskii, E. V., and Entin, S. D., *Kinet. Katal.* **13**(2), 933 (1972).
9. Nagakura, S., *J. Phys. Soc. Japan* **14,** 186 (1959).
10. Anderson, R. B., *in* "Catalysis" (P. H. Emmett, Ed.), Vol. IV, pp. 1–371. Reinhold, New York, 1956.

11. Pichler, H., *in* "Advances in Catalysis and Related Subjects" (W. G. Frankenburg, V. I., Komarewsky, and E. K. Rideal, Eds.), Vol. 4, p. 271. Academic Press, New York, 1952.
12. Hansen, M., "Constitution of Binary Alloys," 2nd ed. McGraw–Hill, New York, 1958.
13. Hofer, L. J. E., Sterling, E., and McCartney, J. T., *J. Phys. Chem.* **59,** 1153 (1955).
14. Tøttrup, P. B., *J. Catal.* **42,** 29 (1976).
15. Goldschmidt, H. J., "Interstitial Alloys." Plenum, New York, 1967.
16. Dwyer, D., Yoshida, K., and Somorjai, G. A., *Amer. Chem Soc. Div. Petrol. Chem. Preprints* **23**(2), 521 (1978).
17. Wentrcek, P. R., Wood, B. J., and Wise, H., *J. Catal.* **43,** 363 (1976).
18. Storch, H. H., Golumbic, N., and Anderson, R. B., "The Fischer-Tropsch and Related Syntheses." Wiley, New York, 1951.
19. Hofer, L. J. E., *in* "Catalysis" (P. H. Emmett, Ed.), Vol. IV, pp. 373–441. Reinhold, New York, 1956.
20. Rostrup-Nielsen, J. R., Jr., *J. Catal.* **33,** 184 (1974).
21. Amenomiya, Y., and Cvetanovic, R. J., *J. Phys. Chem.* **67,** 144, 2046, 2705 (1963).
22. Falconer, J. C., and Madix, R. J., *Surface Sci.* **48,** 393 (1975).
23. Rozovskii, A. Y., Biryukovich, M. M., Ivanov, A. A., Kagan, Y. B., and Bashkirov, A. N., *Kinet. Katal.* **4,** 373 (1963).
24. Askill, J., "Tracer Diffusion Data for Metals, Alloys, and Simple Oxides." Plenum, New York, 1970.
25. Kryukov, Y. B., Bashkirov, A. N., Liberov, L. G., and Fridman, R. E., *Kinet Katal.* **12**(1), 107 (1971).
26. Araki, M., and Ponec, V., *J. Catal.* **44,** 439 (1976).
27. Ford, R. R., *in* "Advances in Catalysis and Related Subjects" (D. D. Eley, H. Pines, and P. B. Weisz, Eds.), Vol. 21, p. 51. Academic Press, New York, 1970.
28. Textor, M., Gay, I. D., and Mason, R., *Proc. Roy. Soc. London Ser. A* **356,** 37 (1977).
29. Kryukov, Y. B., Bashkirov, A. N., Liberov, L. G., Butyugin, V. K., and Stepanova, N. D., *Kinet. Katal.* **2**(5), 780 (1961).